# Journal Pre-proof


The influence of the starch coating on the magnetic properties of nanosized cobalt ferrites obtained by different synthetic methods

Marija Šuljagić (Methodology) (Investigation) (Writing - original draft), Predrag Vulić (Investigation) (Writing - original draft), Dejan Jeremić (Investigation) (Writing - original draft), Vladimir Pavlović (Investigation) (Writing - original draft), Suzana Filipović (Investigation) (Writing - original draft), Lukasz Kilanski (Conceptualization) (Investigation) (Writing - original draft) (Writing - review and editing), Sabina Lewinska (Investigation) (Writing - original draft), Anna Slawska-Waniewska (Investigation) (Writing - original draft), Milica R. Milenković (Investigation) (Writing - original draft), Aleksandar S. Nikolić (Investigation) (Writing - original draft), Ljubica Andjelković (Conceptualization) (Methodology) (Investigation) (Writing - original draft) (Writing - review and editing) (Supervision)

PII: S0025-5408(20)31598-1

DOI: https://doi.org/10.1016/j.materresbull.2020.111117

Reference: MRB 111117

To appear in: *Materials Research Bulletin*

Received Date: 12 May 2020

Revised Date: 8 October 2020

Accepted Date: 19 October 2020

Please cite this article as: { doi: https://doi.org/

# The influence of the starch coating on the magnetic properties of nanosized cobalt ferrites obtained by different synthetic methods

Marija Šuljagić,[1] Predrag Vulić,[2†] Dejan Jeremić,[3] Vladimir Pavlović,[4,5] Suzana Filipović,[5] Lukasz Kilanski,[6*] Sabina Lewinska,[6] Anna Slawska-Waniewska,[6] Milica R. Milenković,[7] Aleksandar S. Nikolić,[7] Ljubica Andjelković[1*]

[1]University of Belgrade, Institute of Chemistry, Technology and Metallurgy, Department of Chemistry, Njegoševa 12, 11000 Belgrade, Republic of Serbia,
e-mail: ljubica@chem.bg.ac.rs (L. A.), marija.suljagic@ihtm.bg.ac.rs (M. Š.)
[2]Faculty of Mining and Geology, University of Belgrade, Djušina 7, 11000 Belgrade, Serbia,
e-mail: predrag.vulic@rgf.bg.ac.rs
[3]Innovation Center of the Faculty of Chemistry, University of Belgrade, Studentski Trg 12–16, 11000 Belgrade, Serbia, e-mail: djeremic@chem.bg.ac.rs
[4]Faculty of Agriculture, University of Belgrade, Belgrade, 11000, Serbia,
e-mail: vladimirboskopavlovic@gmail.com
[5]Institute of Technical Sciences of SASA, Knez Mihailova 35/IV, Belgrade, 11000, Serbia,
e-mail: suzana.filipovic@itn.sanu.ac.rs
[6]Institute of Physics, Polish Academy of Sciences, Aleja Lotnikow 32/46, PL-02668 Warsaw, Poland, e-mail: kilan@ifpan.edu.pl (L. K.), lewinska@ifpan.edu.pl (S. L.), slaws@ifpan.edu.pl (A. S. W.)
[7]Faculty of Chemistry, University of Belgrade, Studentski Trg 12-16, 11000 Belgrade, Serbia,
e-mail: mrm@chem.bg.ac.rs (M. R. M.), asn@chem.bg.ac.rs (A. S. N.)

*Corresponding authors
† 1973-2020

Graphical abstract

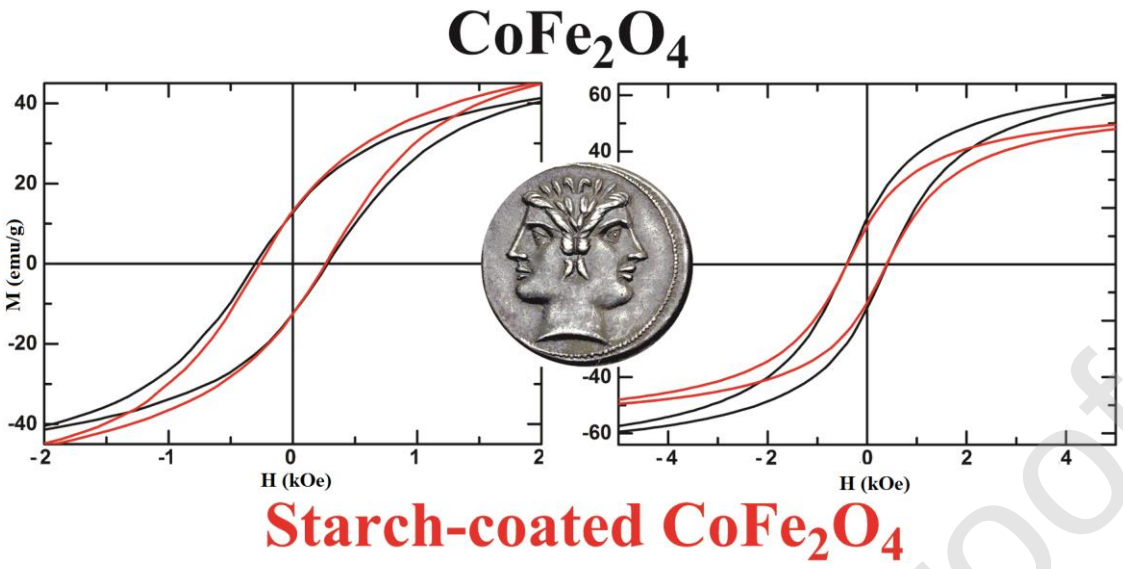


**Highlights**

- Nanostructured cobalt ferrites' magnetic properties
- “Janus effect” of starch coating on cobalt ferrite magnetization
- Co-precipitation and hydrothermal methods/starch coating – increased magnetization
- Mechanochemical and microemulsion methods/starch coating – decreased magnetization

**Abstract**

To investigate the magnetic behavior of starch-coated cobalt ferrites, well-established synthetic methods, i.e., coprecipitation, mechanochemical, ultrasonically assisted coprecipitation, microemulsion, and microwave-assisted hydrothermal syntheses were chosen for their preparation. The obtained materials had pure single-phase spinel structures. Scanning and transmission electron microscopy analyses revealed that the morphology of the samples is not uniform, and particle aggregation is a dominant process. Fourier transform infrared spectra and thermogravimetric analysis confirmed the presence of starch in all–coated samples. The unusually higher saturation magnetization of starch-coated samples than their as-prepared analogs, obtained by coprecipitation, ultrasonically assisted coprecipitation, and microwave-

assisted hydrothermal methods, might be explained by the Ostwald ripening mechanism induced by the coating process. A decrease in magnetization was noticed for the starch-functionalized nanomaterials synthesized by mechanochemical and microemulsion methods, in comparison to their as-prepared analogs, i.e., the size distribution of such nanoparticles is narrow, and the average diameter of the grains is near critical for the Ostwald ripening process.

**Keywords:** A. magnetic materials, A. oxides, A. nanostructures, B. chemical synthesis, B. magnetic properties

## 1. Introduction

Stable suspensions of magnetic nanoparticles (MNPs), *aka* ferrofluids, initially developed for technological applications [1-3], recently became materials with an impact in the fields of analytical chemistry, biosensing, and nanomedicine [4-11]. Rapid development in the design of MNPs with desired properties of size, morphology, chemical composition, and surface chemistry requires a multidisciplinary point of view, both from the chemistry associated with the challenging synthetic methods and the physics utilized for the determination and optimization of their magnetic properties [12]. Magnetism is an important prerequisite to employ nanoparticles as building blocks for different biological applications: as contrast agents for magnetic resonance imaging (MRI), for bio-assays using magnetic separation, as internal heat sources for thermoablation of tumors, as drug carriers with magnetic guiding capability, for targeted drug release activated by an applied magnetic field and theranostic agents [5, 6, 13-16]. Functional nanoparticles in the sub-100 nm regime with controlled shapes and morphologies, mostly due to their size, can penetrate cell walls and deliver drugs for diagnostic and therapeutic purposes in an efficient manner. Moreover, regarding hyperthermia, a uniform distribution of nanoparticles determines a well-controlled temperature increase in tumor tissue. Applications of MNPs in the biomedical field are limited by the biocompatibility and colloidal stability of the nanoparticles. This can be overcome by proper layering and capping using surface layers of polymers, silica, functionalized long-chain organic molecules, etc. [17-23]. Biocompatible shells can be designed to target different molecules. However, to tailor properties such as surface area, particle size presents the major precondition. The literature is rife with controlled size and shape chemical preparation methods of MNPs [24-29]. Generally, the size of nanoparticles is strongly affected by the boiling point of the solvent [30], reaction time [31], and annealing conditions [32, 33],

while their shape is usually tuned by varying the heating rate [34], the precursor/surfactant ratio [35], the reaction time or the concentrations of the reagents [36, 37].

Among the many magnetic materials, cobalt ferrite ($CoFe_2O_4$), with a cubic-closest-packed inverse spinel structure, has attracted great attention due to its unique magnetic, electronic, optical and physical properties, such as chemical and thermal stabilities, large magnetocrystalline anisotropy, high Curie temperature and high coercivity at room temperature. These outstanding properties make $CoFe_2O_4$ a promising and suitable candidate for a large variety of different medical applications [38-40]. A plethora of different synthesis procedures have been developed to produce $CoFe_2O_4$ nanoparticles with improved physical and chemical properties [34, 37, 41-55]. However, some preparation procedures may result in very small particles with poor magnetic properties, wide particle distributions, nonstoichiometric ferrites and the presence of nonmagnetic iron oxide phases. Small sizes can somewise be eliminated by annealing over 600 °C [47]. On the other hand, possible sintering may lead to particle sizes larger than the critical size for single-domain behavior and restrict surface modification. Furthermore, the production of ferrites with a pure spinel phase in some cases requires annealing treatment [56].

In this study, stoichiometric $CoFe_2O_4$ MNPs were synthesized by five different preparation techniques, i.e., coprecipitation, ultrasonically assisted coprecipitation, mechanochemical, microwave-assisted hydrothermal, and microemulsion syntheses. These methods were chosen for their fast performance, simplicity, reproducibility, and scalability. Moreover, such techniques are well known to the scientific community as preparation methods of MNPs with desired performances. To obtain stable and biocompatible colloids necessary for possible medical applications, all magnetic cores were coated with starch, a strongly hydrophilic and biodegradable natural compound. Starch interacts with the surface of the MNPs through hydroxylic (R-OH) groups, resulting in a relatively weakly bonded coating provided by electrostatic interactions in a colloidal assembly [57]. The crystallinity, morphology, and chemical composition of these MNPs were studied using X-ray powder diffraction, scanning electron microscopy, energy-dispersive X-ray spectroscopy, and transmission electron microscopy. The magnetic properties of all samples were measured and discussed. The effects of starch coating on the magnetization of $CoFe_2O_4$ nanoparticles were clarified, giving rise to magnetically driven applications.

## 2. Material and Methods

### 2.1 Materials

All chemicals (iron (III) chloride hexahydrate ($FeCl_3 \cdot 6H_2O$, 98%), cobalt (II) chloride hexahydrate ($CoCl_2 \cdot 6H_2O$, 98%), sodium hydroxide (NaOH, >97%), cetyltrimethylammonium bromide (CTAB, >98%), n-butanol (99.8%), n-hexanol (>99%), iron(III) nitrate nonahydrate ($Fe(NO_3)_3 \cdot 9H_2O$, >99.95), cobalt(II) nitrate hexahydrate ($Co(NO_3)_2 \cdot 6H_2O$, >99.99), ammonium hydroxide solution (28% $NH_3$ in water), absolute ethanol and soluble starch) were obtained from Sigma-Aldrich (p.a. quality) and used without additional purification. Deionized water was used in these experiments.

## 3. Experimental

### 3.1 Coprecipitation synthesis

The sample was synthesized using 0.02 mol $Fe^{3+}$ and 0.01 mol $Co^{2+}$ chlorides as precursors by dissolving them in 50 mL of deionized water and then heating to boiling. To ensure complete precipitation of cobalt and iron cations, excess 1 M NaOH solution was rapidly added with constant stirring. The appearance of a black precipitate was noted, and the pH value of the solution was 11. The reaction mixture was refluxed for 1 hour. The mixture was cooled to room temperature and filtered. The precipitate was washed with distilled water until the excess hydroxide was completely removed (neutral pH), separated from the solution using vacuum filtration, and dried at 100 °C for 2 hours. Furthermore, the powder was divided into two equal parts. The first part was pulverized in an agate mortar and annealed in an electrical furnace with a heating rate of 10 °C/min at $T$ = 450 °C for 1 hour. The second part was transferred to the planetary mill.

### 3.2 Mechanochemical synthesis

Mechanochemical treatment was performed in a planetary ball mill (Retsch PM100CM). A hardened-steel vial (500 $cm^3$ volume) filled with 10 hardened-steel balls (8 mm in diameter) was used as the milling medium. The powder prepared by the coprecipitation method was ball-milled for 10 h at 500 rpm in closed hardened steel containers with a ball-to-sample mass ratio of 20:1. The angular velocities of the supporting disc and vial were 32.2 and 40.3 rad $s^{-1}$, respectively. The intensity of milling corresponded to an acceleration of approximately 10 times the

gravitational acceleration.

### 3.3 Ultrasonically assisted coprecipitation synthesis

Solutions of $CoCl_2 \cdot 6\ H_2O$ and $FeCl_3 \cdot 6\ H_2O$ were mixed in their stoichiometric ratio. The concentrations of $Fe^{3+}$ and $Co^{2+}$ were 0.4 M and 0.2 M, respectively. The final volume of solution was 50 mL. To this end, excess 1 M NaOH was rapidly added with constant stirring. The pH of the solution was maintained at 11. The mixture was then heated at 80 °C and ultrasonically treated for approximately 1 hour. The precipitated particles were then washed several times with deionized water to remove the hydroxide residues and other impurities, and separated from the solution using vacuum filtration. The precipitate was further dried at 80 °C, followed by pulverization in the agate mortar and annealing in the electrical furnace as the sample obtained by coprecipitation (section 2.2.1).

### 3.4 Microemulsion synthesis

A microemulsion system with CTAB as the surfactant, n-butanol as the cosurfactant, n-hexanol as the oil phase and an aqueous solution as the water phase was chosen. The microemulsion contained 15 wt% hexanol and 45 wt% aqueous solution, and surfactant to cosurfactant ratio was 60/40. Two microemulsions with identical compositions but different aqueous phases were prepared. The first microemulsion contained aqueous solutions of a stoichiometric amount of $Fe^{3+}$ and $Co^{2+}$ nitrates, whereas the second microemulsion contained an aqueous solution of the precipitation agent ammonium hydroxide. These two microemulsions were then mixed under constant stirring and heated for 1 hour at 90 °C. The pH value after precipitation was approximately 11. The microemulsion with the product nanoparticles was mixed with a water/ethanol mixture and precipitated by centrifugation. Finally, the precipitate was washed with absolute ethanol to remove any oil and surfactant residues from the particles, separated from the solution using vacuum filtration, and dried at 70 °C. The precipitate was pulverized in the agate mortar and annealed in the electrical furnace under the conditions provided in section 2.2.1.

### 3.5 Microwave-assisted hydrothermal synthesis

Stoichiometric amounts of chloride salts of $Fe^{3+}$ and $Co^{2+}$ necessary to prepare 1.5 g of $CoFe_2O_4$ were dissolved in deionized water. Afterwards, a small excess of ammonium hydroxide was

added. The pH value was approximately 10. The overall volume of the mixture was divided into seven vessels, each with a volume of 100 mL. Each vessel contained 50 mL of the mixture. The vessels were placed in an HPR-1000/10S high pressure segmented rotor and heated in the microwave digester (ETHOS 1, Advanced Microwave Digestion System, MILESTONE, Italy). The power of microwave irradiation was set in the range of 0-1000 W, with linear heating of the mixture at 20 °C/min. The mixture was then heated at 200 °C for 20 minutes at a maximum pressure of 100 bars. Subsequently, the vessels were cooled in air. The prepared particles were separated from the solution using vacuum filtration. The precipitate was then washed several times with deionized water to remove excess chlorides. The synthesized nanoparticles were dried at 70 °C for one day. After drying, the residue was pulverized in the agate mortar.

### 3.6 Functionalization with starch

With the aid of ultrasound, 0.5 g of $CoFe_2O_4$ powder was dispersed in deionized water (20 mL). First, 2.5 g of starch was dissolved in boiling water, and 200 mL of 2 M NaOH solution was prepared. Then, the starch solution and ferrite dispersions were mixed and added dropwise in hydroxide solutions. The obtained mixtures were ultrasonically treated for 1 hour at 80 °C. Afterwards, the samples were cooled to room temperature, washed with deionized water to remove excess starch and hydroxide, and separated from the solution using vacuum filtration. The samples were dried for 48 hours at room temperature.

### 3.7 Characterizations

XRPD patterns for all of the samples were collected using a Rigaku SmartLab automated powder X-ray diffractometer with Cu $K\alpha_1$ ($\lambda$ = 1.54059 Å) radiation ($U$ = 40 kV, $I$ = 30 mA) equipped with a D/teX Ultra 250 stripped 1D detector in the XRF reduction mode. The diffraction angle range was 15 – 90 °2θ with a step of 0.01 ° at a scan speed of 2 °/min. Structural and microstructural investigations of all samples (cobalt ferrites and starch-coated cobalt ferrites) were conducted by the Rietveld method, as implemented in dedicated Rigaku PDXL2.0 software and based on the fundamental parameters approach (FPA) [58].

Scanning electron microscopy (SEM) and energy-dispersive X-ray spectroscopy (EDS) analyses were performed with a JEOL JSM-6610LV scanning electron microscope. EDS analyses were conducted in the area of $1 \times 10^4$ $\mu m^2$ per sample. Transmission electron microscopy (TEM) analysis was performed on a JEOL JEM-1400 Plus electron microscope with a voltage of 120 kV

and a LaB6 filament at different magnifications appropriate for observation of aggregation details.

The Fourier transform IR (FT-IR) spectra were recorded on a Nicolet 6700 FT-IR instrument (Thermo Scientific) in the range of 4000 – 400 $cm^{-1}$ using the ATR technique with a Smart Orbit accessory (diamond crystal). The accuracy of FTIR is 4 $cm^{-1}$. The uncertainty of the method with a 95% confidence interval is 0.2 $cm^{-1}$ obtained for 20 independent measurements of the band at 1601.2 $cm^{-1}$ that originates from the certified polystyrene standard. The number of scans for IR sample measurements was 32, while the number of scans for background measurements was 16.

Thermogravimetric analysis (TGA) and differential thermal analysis (DTA) of the as-prepared and starch-coated $CoFe_2O_4$ nanoparticles were performed by a Thermogravimetric Analyzer TA SDT 2960 (TA Instruments, New Castle, DE USA). All TGA and DTA experiments were conducted in synthetic air (99.999%) with a purge flow of 80 mL/min. The applied temperature was changed from room temperature to 700 °C at a heating rate of 15 °C/min.

Magnetic measurements were performed using a commercial Quantum Design Physical Property Measurement System (PPMS) equipped with a 9 T superconducting magnet and a vibrating sample magnetometer (VSM) option. Temperature dependences of the magnetization, *M(T)*, were measured upon heating in the zero-field cooled (ZFC) and the field-cooled (FC) regime at 100 Oe from 5 to 300 K. Hysteresis loops, *M(H)*, were measured at 300 K in the field range ±9 T.

## 4. Results and Discussion

The X-ray powder patterns of samples prepared by five different synthesis routes are shown in Figure 1. The diffraction maxima present in the XRPD patterns were identified by ICDD PDF2 file number 22-1086. It is obvious that, for both types of samples, as-prepared and coated, a single spinel phase is present. The formation of pure $CoFe_2O_4$ is confirmed in all cases with no detectable residual phase of hematite. The XRPD patterns show peaks with considerable broadening, indicating the small crystallite size of the ferrite powders. To evaluate the quality of the Rietveld refinement, the weighted profile R-factor ($R_{wp}$), the unweighted profile R-factor ($R_p$), the statistically expected R value ($R_{exp}$) and $\chi^2$ value are presented in Table 1. The calculated values of the unit cell parameter (Å), volume ($Å^3$), crystallite size (Å) and microstrain (%) of the prepared particles are given in Table 2. The obtained unit cell parameters are

comparable to the values reported in the literature [59]. However, the largest unit cell volume and unit cell parameters were registered for the mechanochemically prepared $CoFe_2O_4$. For the as-prepared samples obtained by wet chemical routes, the particles prepared with the aid of ultrasound have the smallest crystallite size, while the crystallites obtained by the microemulsion method are the largest. For the same annealing conditions, the crystallite sizes in the samples slightly differ from each other, which reflects the strong effect of the synthesis method. The crystallite size is related to the relative interdependence between the nucleation and growth steps, and it is strongly influenced by the preparation method. This indicates that the nucleation rate was higher than the growth rate in the ultrasonically treated samples compared to the other annealed powders. In starch-coated samples, the crystallite size slightly increases. The microstrain values for the uncoated and corresponding-coated samples are similar. Among all investigated powders, the microstrain value is the smallest for the $CoFe_2O_4$ prepared by the microemulsion method due to the lowest temperature of preparation.

In all investigated samples, EDS analyses corroborate divalent cobalt and trivalent iron stoichiometric ratios close to 1:2 (Table 3). SEM analysis was performed to visualize the morphology of the synthesized magnetic nanoparticles. According to the SEM results (Figure 2), the synthesized particles have a significant tendency to agglomerate due to their ferrimagnetic nature. Furthermore, smaller agglomerates from 150 to 400 nm and larger with dimensions of approximately 0.7-1.5 μm were observed. To obtain a more detailed picture of the microstructure of the synthesized powders, TEM measurements were performed. The recorded TEM micrographs are presented in Figure 3. The general observation is that the morphologies of the samples are not uniform, and aggregations of individual particles are the dominant process in all monitored samples. Two kinds of particles are observed in the presented micrographs, larger polygonal and smaller particles with almost spherical shapes. The polygonal particles are larger than 20 nm, while smaller particles are in the range of 10-20 nm. The structure of smaller particles gravitates to amorphous, in contrast to polygonal ones. This could be explained by the mechanism of crystalline $CoFe_2O_4$ formation. In the first step of the chemical reaction, amorphous $CoFe_2O_4$ was formed, and, during the heat treatment, the reaction propagated along with crystallization and grain growth. It was shown in the literature that, for this type of material, changes in morphology are observed [60] throughout grain growth. From the TEM images of the

starch-coated powders (right side of Figure 3), encapsulation of individual particles cannot be observed. Thus, conclusions about changes in particle size cannot be made.

FT-IR spectra of as-prepared and coated particles, taken in the range of 4000 to 400 $cm^{-1}$ are presented in Figure 4. The exact wavenumbers and band assignments are given in Table 4. The fingerprint region of the FT-IR spectra showed M–O (M = Co, Fe) stretching modes of spinel ferrites, i.e., two characteristic vibrational modes for the spinel structure at approximately 570 $cm^{-1}$ and 420 $cm^{-1}$ are present in all investigated samples. The strong band corroborated stretching vibrations of $Fe^{3+}$ ion at a tetrahedral site ($Fe_{tetra}$–O), while the band of weaker intensity originated from $Co^{2+}$ vibrations at an octahedral site ($Co_{octa}$–O). Free or absorbed water in the samples caused the appearance of two peaks near 3360 and 1630 $cm^{-1}$. The FT-IR spectra given in Figure 4b confirmed the attachment of starch moieties, i.e., five bands at approximately 2930, 1450, 1340, 1000 and 920 $cm^{-1}$ typical for starch can be observed [21, 61]. The weak band at approximately 2930 $cm^{-1}$ can be assigned to stretching vibrations of -$CH_2$ and -CH groups, while the signals near 1450 and 1340 $cm^{-1}$ are connected to their bending vibrations. The band corresponding to 1000 $cm^{-1}$ represents the C-OH stretching mode. The absorption peak at 920 $cm^{-1}$ is due to stretching vibrations of glycosidic linkages (C-O-C) [21]. Therefore, FT-IR spectra confirmed the presence of starch in all investigated coated samples.

TG and DT analyses were performed to determine the amount of starch in the coated $CoFe_2O_4$ samples and all the transformations that have occurred (Figure 5 and Figure 6). DT curves show two characteristic peaks that can be attributed to the endothermic process of free or adsorbed water evaporation and the exothermic process of organic layer combustion (starch-coated samples). According to the TG and DTG curves for the as-prepared and starch-coated samples, weight loss between 1% and 3% was noted at 200 °C for the starch-coated samples (Figure 6). Even though the coating procedure includes the usage of high starch concentrations, these results indicate that the amount of starch attached to the $CoFe_2O_4$ particle surfaces is very low.

Figure 7 shows the temperature (left side) and magnetic field (right side) dependences of the magnetization, *M*, for both, the as-prepared and starch-coated $CoFe_2O_4$ samples measured using the PPMS platform.

The left part of Figure 7 presents the temperature dependences of the magnetization measured in the zero-field-cooled (ZFC) and field-cooled (FC) regimes at the applied field of 100 Oe for all investigated samples. All measured ZFC-FC relations have similar curvatures. The ZFC relations do not exhibit any extrema, and the magnetization increases with temperature from 5 to 300 K. All FC curves are nearly constant over the abovementioned temperature range. With the introduction of starch, nonsystematic changes in the magnetization values of the ZFC-FC relations are observed with respect to the uncoated samples. In the case of the samples prepared using coprecipitation and ultrasonically assisted coprecipitation methods, the $M(T)$ curves showed higher values for the starch-coated nanoparticles. In contrast, for the $CoFe_2O_4$ nanoparticles prepared using mechanochemical and microemulsion methods, the $M(T)$ curves for the as-prepared samples have larger values than those for the starch-coated samples. It should also be noted that the smallest differences between the $M(T)$ curves for the as-prepared and coated samples were observed for the samples obtained with the microwave-assisted hydrothermal method. Figure 7 also shows that, for the starch-coated sample prepared by the microemulsion method, the ZFC curve obtained negative values below 200 K.
On the right side of Figure 7, a set of magnetization measurements as a function of the magnetic field obtained at $T$ = 300 K for both the as-prepared and starch-coated $CoFe_2O_4$ nanoparticle samples is presented. All the $M(H)$ curves exhibit different and nonzero coercive field values, $H_C$, and different values of the magnetization at 90 kOe, here called the $M_S$ (Table 5). Similar to the ZFC-FC relations, the $M_S$ values after starch coating do not exhibit systematic changes. For the samples prepared by coprecipitation, ultrasonically assisted coprecipitation and microwave assisted hydrothermal methods $M_S$ increased by ca. 5-7% compared to the samples without coating. For the two remaining samples, the starch coating caused the reduction of $M_S$ at levels near 10 and 18%.

In Figure 7, $M/M_S(H)$ relations are also plotted. It should be noted that the best overlap between hysteresis loops measured for pairs of the as-prepared and coated samples is observed for

microemulsion samples. Additionally, for the pairs of the samples made by mechanochemical and microwave-assisted hydrothermal methods, the curvature differences in $M/M_S(H)$ are very slight but noticeable below 20 kOe. The most significant variation in the curvature of $M/M_S(H)$ relations for as-prepared and coated samples is highly visible for the materials obtained by coprecipitation and ultrasonically assisted coprecipitation methods – the loops for samples without and with starch do not overlap below 30 kOe.

Comparable ZFC-FC relations (without visible maximum in the ZFC curve and nearly constant in the temperature value of the FC curve up to 300 K) were observed earlier for cobalt ferrite nanoparticles [52, 62]. Kim et al. explained the registered ZFC relation based on Mössbauer spectra for 15 nm $CoFe_2O_4$ nanoparticles synthesized by the temperature-controlled coprecipitation method [62]. The authors predicted that their sample up to 550 °C is composed of superparamagnetic and ferromagnetic fractions; thus, the maximum in the ZFC curve is not registered, and a nonzero $H_C$ at 300 K is observed [62]. However, this explanation is hard to relate to our results without Mössbauer studies. As shown in Figures 2 and 3, synthesized $CoFe_2O_4$ nanoparticles with and without starch coatings are agglomerated systems. In such systems, grains are very close to each other, and it is expected that interactions between them are significant and have an influence on the macroscopic magnetic properties [63]. In our studies, the presence of the starch shell should reduce the strength of the interparticle interactions due to an increase in the distances between the nanoparticles; thus, the theoretical value of the shell thickness was calculated. Knowing the mass percentage of the starch in the coated samples, it is possible to evaluate the thickness of starch shells. Taking into account the densities of cobalt ferrite ($\rho(CoFe_2O_4)$=5.3 g/cm$^3$) and starch ($\rho$(starch)=1.5 g/cm$^3$) and approximately spherical 15 nm diameter $CoFe_2O_4$ nanoparticles as the core, the thickness of the shell can be estimated as a value between 0.1 and 0.3 nm, depending on the starch concentration. Such values of the shell thickness indicate that the starch coating in the investigated samples has rather island-like character and cannot cover the single nanoparticle completely. Also taking into account the $M(T)$ data gathered in Figure 7, where the ZFC-FC relations for the uncoated and coated samples have similar curvatures, the presence of magnetic interactions between the magnetic nanoparticles in all investigated samples seems to be obvious.

The obtained $M_S$ values (at 300 K) for all discussed samples are lower than 80 emu/g, which is expected for bulk $CoFe_2O_4$ [64]. The observed reduction of the saturation magnetization with

regard to the bulk value is probably related to the near-surface layer, where the disorder of the magnetic moments is possible [63, 65, 66]. Notably, for the samples prepared using mechanochemical and microemulsion methods, the observed decrease in $M_S$ after starch coating is consistent with theoretical predictions and the literature [67, 68]. It is well known that starch is a diamagnetic material; therefore, covering $CoFe_2O_4$ nanoparticles with it should lead to a decrease in magnetization per mass unit. In the case of some samples, and especially for the case of the starch-coated sample prepared by the microemulsion method, where the ZFC curve obtained negative values below 200 K, the reason for the observed reduction of the magnetization may have an additional origin. The negative magnetization observed in this sample can be related to the presence of a small negative residual field of the superconducting magnet during cooling from room temperature to 2 K before the ZFC measurement.

For the samples prepared by coprecipitation, ultrasonically assisted coprecipitation and microwave-assisted hydrothermal methods, $M_S$ values registered after the starch coating gave unexpected results – the increase of $M_S$ – it is quite possible that ultrasound used during the coating procedure can destroy smaller aggregates in the synthesized samples, and rearrangement of the particles by the Ostwald mechanism (also called coarsening) can occur. There is no direct but possible correlation between the Ostwald ripening process and $M_S$ value. In the Ostwald ripening process, larger particles enhance their diameters at the expense of smaller ones, resulting in the shift of the particle distribution to higher diameter values. This mechanism is related to the thermodynamic stability of the system, i.e., smaller particles have higher solubility than larger particles [69, 70]. It is known that, in nanoparticle systems, $M_S$ values increase with the diameter of particles [47, 71, 72]. Thus, if during the starch coating process, the average diameter of nanoparticles increases by the Ostwald mechanism, the enhancement of the $M_S$ value after coating becomes possible. It should be noted that the potential presence of a coarsening process for the samples prepared by coprecipitation, ultrasonically assisted coprecipitation and microwave-assisted hydrothermal methods does not exclude the existence of the starch coating. Most likely, the increase in the $M_S$ value induced by the enhancement of the average particle dimensions in these three samples is more significant than the reduction in the $M_S$ value after the functionalization of nanoparticles. The Ostwald ripening process takes place only if particles with diameters below the critical radius exist in the system. This critical radius is connected with the solubility of the particles. If the particles have dimensions equal to or above the critical

diameter, the process does not take place. In this context, we suppose that, for the samples made by mechanochemical and microemulsion methods, the size distribution of nanoparticles is narrow, and the average grain size is near critical for the Ostwald ripening process; thus, the influence of coarsening is not as significant as in the case of the three other samples [70].

## 5. Conclusion

To demonstrate how $CoFe_2O_4$ structures and ultrasonically assisted starch coatings are intertwined with the resulting magnetic properties, five different synthesis methods were performed. The XRPD patterns for all investigated samples revealed characteristic peaks for the pure spinel structure. According to the SEM and TEM data, the presence of highly agglomerated nanometric $CoFe_2O_4$ powders was confirmed. The FT-IR results clearly indicate the presence of starch. Attention should be paid to the fact that examined samples may be divided into two main groups. Starch functionalization of the samples prepared by coprecipitation, ultrasonically assisted coprecipitation and microwave-assisted hydrothermal methods resulted in a slight increase in the $M_S$ value. The curvature of hysteresis loops changed after the coating process, especially for the samples obtained by coprecipitation and ultrasonically assisted coprecipitation methods, opening new perspectives for –OH-based coatings of nanoparticles for applications in biomedicine. These unexpected magnetic properties are linked to the Ostwald ripening process, i.e., the diffusion of smaller particles onto larger particles was probably caused by ultrasound assistance during the coating procedure. It should be noted that this hypothesis does not exclude existence of the starch in samples prepared by the coprecipitation, ultrasonically assisted coprecipitation, and microwave-assisted hydrothermal methods.

In the second group, where samples prepared by mechanochemical and microemulsion methods can be assigned, the theoretically predicted decrease in the $M_S$ value was occured. The observed decrease in $M_S$ values after starch coating is a consequence of the reduction in the content of the magnetic component for these two samples. However, the magnetic properties of coated nanoparticles synthesized by mechanochemical and microemulsion methods, as well as their narrow size distribution, give us confidence for their further medical applications.

Finally, the magnetic properties of ferrite-based nanomaterials, dependent on the physical parameters, such as size, shape, composition, and core-shell architecture, can be selectively and judiciously tuned by the proper choice of the synthesis route.

## Author statement

Authors have contributed in multiple roles.

**Marija Šuljagić:** Methodology; Investigation; Writing - Original Draft

**Predrag Vulić:** Investigation; Writing - Original Draft

**Dejan Jeremić:** Investigation; Writing - Original Draft

**Vladimir Pavlović:** Investigation; Writing - Original Draft

**Suzana Filipović:** Investigation; Writing - Original Draft

**Lukasz Kilanski:** Conceptualization; Investigation; Writing - Original Draft; Writing - Review & Editing

**Sabina Lewinska:** Investigation; Writing - Original Draft

**Anna Slawska-Waniewska:** Investigation; Writing - Original Draft

**Milica R. Milenković:** Investigation; Writing - Original Draft

**Aleksandar S. Nikolić:** Investigation; Writing - Original Draft

**Ljubica Andjelković:** Conceptualization; Methodology; Investigation; Writing - Original Draft; Writing - Review & Editing; Supervision

**Declaration of interests**

☒ The authors declare that they have no known competing financial interests or personal relationships that could have appeared to influence the work reported in this paper.

**Acknowledgments**

This work was financially supported by the Serbian Ministry of Education, Science and Technological Development (Grant No. 451-03-68/2020-14/200026). Ljubica Andjelković acknowledges “Startup for Science, Serbia” 2017/18.

This paper is dedicated to the memory of our friend and colleague, Predrag Vulić.

**References**

[1] Jeong U, Teng X, Wang Y, *et al*. Superparamagnetic Colloids: Controlled Synthesis and Niche Applications. *Adv Mater* 2007, **19**: 33-60.

[2] Lu AH, Salabas EL, Schüth F. Magnetic Nanoparticles: Synthesis, Protection, Functionalization, and Application. *Angew Chem Int Ed* 2007, **46**: 1222-1244.

[3] Park BJ, Fang FF, Choi HJ. Magnetorheology: materials and application, *Soft Matter* 2010, **6**: 5246-5253.

[4] Pankhurst QA, Connolly J, Jones SK, Dobson J. Applications of magnetic nanoparticles in biomedicine. *J Phys D* 2003, **36**: R167.

[5] Corot C, Robert P, Idée JM, Port M. Recent advances in iron oxide nanocrystal technology for medical imaging. *Adv Drug Deliv Rev* 2006, **58**: 1471-1504.

[6] Hervault A, Thanh NTK. Magnetic nanoparticle-based therapeutic agents for thermo-chemotherapy treatment of cancer. *Nanoscale* 2014, **6**: 11553-11573.

[7] Tran N, Webster TJ. Magnetic nanoparticles: biomedical applications and challenges. *J Mater Chem* 2010, **20**: 8760-8767.

[8] Durán JDG, Arias JL, Gallardo V, Delgado AV. Magnetic Colloids As Drug Vehicles. *J Pharm Sci* 2008, **97**: 2948-2983.

[9] Chen Q, Li D, Lin J, *et al*. Simultaneous Separation and Washing of Nonmagnetic Particles in an Inertial Ferrofluid/Water Coflow. *Anal Chem* 2017, **89**: 6915-6920.

[10] Yamaguchi D, Furukawa K, Takasuga M, Watanabe K. A Magnetic Carbon Sorbent for Radioactive Material from the Fukushima Nuclear Accident. *Sci Rep* 2014, **4**:6053.

[11] Mohammed L, Gomaa HG, Ragab D, Zhu J. Magnetic nanoparticles for environmental and biomedical applications: A review. *Particuology* 2017, **30**: 1-14.

[12] Kolhatkar AG, Jamison AC, Litvinov D, *et al*. Tuning the Magnetic Properties of Nanoparticles. *Int J Mol Sci* 2013, **14**: 15977-16009.

[13] Amstad E, Zurcher S, Mashaghi A, *et al*. Surface Functionalization of Single Superparamagnetic Iron Oxide Nanoparticles for Targeted Magnetic Resonance Imaging. *Small* 2009, **5**: 1334-1342.

[14] Chao-Ming F, Yuh-Feng W, Yu-Feng G, *et al*. In vivo bio-distribution of intravenously injected Tc-99 m labeled ferrite nanoparticles bounded with biocompatible medicals. *IEEE Trans Magn* 2005, **41**: 4120-4122.

[15] Chourpa I, Douziech-Eyrolles L, Ngaboni-Okassa L, *et al*. Molecular composition of iron oxide nanoparticles, precursors for magnetic drug targeting, as characterized by confocal Raman microspectroscopy. *Analyst* 2005, **130**: 1395-1403.

[16] Laurent S, Dutz S, Häfeli UO, Mahmoudi M, Magnetic fluid hyperthermia: Focus on superparamagnetic iron oxide nanoparticles, *Adv Colloid Interface Sci* 2011, **166**: 8-23.

[17] Goloverda G, Jackson B, Kidd C, Kolesnichenko V. Synthesis of ultrasmall magnetic iron oxide nanoparticles and study of their colloid and surface chemistry. *J Magn Magn Mater* 2009, **321**: 1372-1376.

[18] Gupta AK, Gupta M. Synthesis and surface engineering of iron oxide nanoparticles for biomedical applications. *Biomaterials* 2005, **26**: 3995-4021.

[19] Sun J, Zhou S, Hou P, *et al*. Synthesis and characterization of biocompatible $Fe_3O_4$ nanoparticles. *J Biomed Mater Res A* 2007, **80A**: 333-341.

[20] Tadmor R, Rosensweig RE, Frey J, Klein J. Resolving the Puzzle of Ferrofluid Dispersants. *Langmuir* 2000, **16**: 9117-9120.

[21] Kim DH, Kim KN, Kim KM, Lee YK. Targeting to carcinoma cells with chitosan- and starch-coated magnetic nanoparticles for magnetic hyperthermia. *J Biomed Mater Res A* 2009, **88A**: 1-11.

[22] Cole AJ, David AE, Wang J, *et al*. Polyethylene glycol modified, cross-linked starch-coated iron oxide nanoparticles for enhanced magnetic tumor targeting. *Biomaterials* 2011, **32**: 2183-2193.

[23] Kim DK, Mikhaylova M, Wang FH, *et al*. Starch-Coated Superparamagnetic Nanoparticles as MR Contrast Agents. *Chem Mater 2003*, **15**: 4343-4351.

[24] Lu LT, Dung NT, Tung LD, *et al*. Synthesis of magnetic cobalt ferrite nanoparticles with controlled morphology, monodispersity and composition: the influence of solvent, surfactant, reductant and synthetic conditions. *Nanoscale* 2015, **7**: 19596-19610.

[25] Chen YX, Chen SP, Zhou ZY, *et al*. Tuning the Shape and Catalytic Activity of Fe Nanocrystals from Rhombic Dodecahedra and Tetragonal Bipyramids to Cubes by Electrochemistry. *J Am Chem Soc* 2009, **131**: 10860-10862.

[26] Xiaohe L, Guanzhou Q, Xingguo L. Shape-controlled synthesis and properties of uniform spinel cobalt oxide nanocubes. *Nanotechnology* 2005, **16**: 3035.

[27] Andrade ÂL, Valente MA, Ferreira JMF, Fabris JD. Preparation of size-controlled nanoparticles of magnetite. *J Magn Magn Mater* 2012, **324**: 1753-1757.

[28] Wang SB, Min YL, Yu SH. Synthesis and Magnetic Properties of Uniform Hematite Nanocubes. *J Phys Chem C* 2007, **111**: 3551-3554.

[29] Baaziz W, Pichon BP, Liu Y, *et al*. Tuning of Synthesis Conditions by Thermal Decomposition toward Core–Shell $Co_xFe_{1-x}O@Co_yFe_{3-y}O_4$ and $CoFe_2O_4$ Nanoparticles with Spherical and Cubic Shapes. *Chem Mater* 2014, **26**: 5063-5073.

[30] Kovalenko MV, Bodnarchuk MI, Lechner RT, *et al*. Fatty Acid Salts as Stabilizers in Size- and Shape-Controlled Nanocrystal Synthesis: The Case of Inverse Spinel Iron Oxide. *J Am Chem Soc* 2007, **129**: 6352-6353.

[31] Yang H., Ogawa T, Hasegawa D, Takahashi M. Synthesis and magnetic properties of monodisperse magnetite nanocubes. *J Appl Phys* 2008, **103**: 07D526.

[32] Hu XC, Capobianchi A, Gallagher R, Hadjipanayis GC. Influence of ball milling and annealing conditions on the properties of L10 FePt nanoparticles fabricated by a new green chemical synthesis method. *J Appl Phys* 2014, **115**: 17A732.

[33] Yeshchenko OA, Dmitruk IM, Dmytruk AM, Alexeenko AA. Influence of annealing conditions on size and optical properties of copper nanoparticles embedded in silica matrix. *Mater Sci Eng B Solid State Mater Adv Technol* 2007, **137**: 247-254.

[34] Song Q, Zhang ZJ. Shape Control and Associated Magnetic Properties of Spinel Cobalt Ferrite Nanocrystals. *J Am Chem Soc* 2004, **126**: 6164-6168.

[35] Zeng H, Rice PM, Wang SX, Sun S. Shape-Controlled Synthesis and Shape-Induced Texture of $MnFe_2O_4$ Nanoparticles. *J Am Chem Soc* 2004, **126**: 11458-11459.

[36] Salazar-Alvarez G, Qin J, Šepelák V, *et al*. Cubic versus Spherical Magnetic Nanoparticles: The Role of Surface Anisotropy. *J Am Chem Soc* 2008, **130**: 13234-13239.

[37] Bao N, Shen L, Padhan P, Gupta A. Self-assembly and magnetic properties of shape-controlled monodisperse $CoFe_2O_4$ nanocrystals. *Appl Phys Lett* 2008, **92**: 173101.

[38] Kim DH, Nikles DE, Johnson DT, Brazel CS, Heat generation of aqueously dispersed $CoFe_2O_4$ nanoparticles as heating agents for magnetically activated drug delivery and hyperthermia. *J Magn Magn Mater* 2008, **320**: 2390-2396.

[39] Lee SW, Bae S, Takemura Y, *et al*. Self-heating characteristics of cobalt ferrite nanoparticles for hyperthermia application. *J Magn Magn Mater* 2007, **310**: 2868-2870.

[40] Joshi HM, Lin YP, Aslam M, *et al*. Effects of Shape and Size of Cobalt Ferrite Nanostructures on Their MRI Contrast and Thermal Activation. *J Phys Chem C* 2009, **113**: 17761-17767.

[41] Cheng F, Peng Z, Liao C, *et al*. Chemical synthesis and magnetic study of nanocrystalline thin films of cobalt spinel ferrites. *Solid State Commun* 1998, **107**: 471-476.

[42] Shi Y, Ding J, Yin H. $CoFe_2O_4$ nanoparticles prepared by the mechanochemical method. *J Alloys Compd* 2000, **308**: 290-295.

[43] Liu Q, Sun J, Long H, *et al*. Hydrothermal synthesis of $CoFe_2O_4$ nanoplatelets and nanoparticles. *Mater Chem Phys* 2008, **108**: 269-273.

[44] S. Sun, H. Zeng, D.B. Robinson, *et al*. Monodisperse $MFe_2O_4$ (M = Fe, Co, Mn) Nanoparticles. *J Am Chem Soc* 2004, **126**: 273-279.

[45] Mathew DS, Juang RS. An overview of the structure and magnetism of spinel ferrite nanoparticles and their synthesis in microemulsions. *Chem Eng J* 2007, **129**: 51-65.

[46] Bao N, Shen L, Wang Y, *et al*. A Facile Thermolysis Route to Monodisperse Ferrite Nanocrystals. *J Am Chem Soc* 2007, **129**: 12374-12375.

[47] Maaz K, Mumtaz A, Hasanain SK, Ceylan A. Synthesis and magnetic properties of cobalt ferrite ($CoFe_2O_4$) nanoparticles prepared by wet chemical route. *J Magn Magn Mater* 2007, **308**: 289-295.

[48] Bao N, Shen L, An W, *et al*. Formation Mechanism and Shape Control of Monodisperse Magnetic $CoFe_2O_4$ Nanocrystals. *Chem Mater* 2009, **21**: 3458-3468.

[49] Bao N, Shen L, Wang YHA, *et al*. Controlled Growth of Monodisperse Self-Supported Superparamagnetic Nanostructures of Spherical and Rod-Like $CoFe_2O_4$ Nanocrystals. *J Am Chem Soc* 2009, **31**: 12900-12901.

[50] Liu XM, Fu SY, Zhu LP. High-yield synthesis and characterization of monodisperse sub-microsized $CoFe_2O_4$ octahedra. *J Solid State Chem* 2007, **180**: 461-466.

[51] Baldi G, Bonacchi D, Innocenti C, *et al*. Cobalt ferrite nanoparticles: The control of the particle size and surface state and their effects on magnetic properties. *J Magn Magn Mater* 2007, **311**: 10-16.

[52] Ognjanović M, Dojčinović B, Fabián M, *et al*. Microwave assisted hydrothermal synthesis of $(Fe,Co)_3O_4$ nanoparticles in the presence of surfactants and effects of Co/Fe ratio on microstructure and magnetism. *Ceram Int* 2018, **44**: 13967-13972.

[53] M. Abbas, B. Parvatheeswara Rao, M. Nazrul Islam *et al*. Size-controlled high magnetization $CoFe_2O_4$ nanospheres and nanocubes using rapid one-pot sonochemical technique. *Ceram Int* 2014, **40**: 3269-3276.

[54] Zhang Y, Yang Z, Yin D, *et al*. Composition and magnetic properties of cobalt ferrite nano-particles prepared by the co-precipitation method. *J Magn Magn Mater* 2010, **322**: 3470-3475.

[55] Pedrosa FJ, Rial J, Golasinski KM, *et al*. Tunable nanocrystalline $CoFe_2O_4$ isotropic powders obtained by co-precipitation and ultrafast ball milling for permanent magnet applications. *RSC Adv* 2016, **6**: 87282-87287.

[56] Ai L, Jiang J. Influence of annealing temperature on the formation, microstructure and magnetic properties of spinel nanocrystalline cobalt ferrites. *Curr Appl Phys* 2010, **10**: 284-288.

[57] Vasilakaki M, Ntallis N, Yaacoub N *et al*. Optimising the magnetic performance of Co ferrite nanoparticles via organic ligand capping. *Nanoscale* 2018, **10**: 21244-21253.

[58] Cheary RW, Coelho A. A fundamental parameters approach to X-ray line-profile fitting. *J Appl Crystallogr* 1992, **25:** 109-121.

[59] Houshiar M, Zebhi F, Razi ZJ, *et al*. Synthesis of cobalt ferrite ($CoFe_2O_4$) nanoparticles using combustion, coprecipitation, and precipitation methods: A comparison study of size, structural, and magnetic properties. *J Magn Magn Mater* 2014, **371**: 43-48.

[60] Phua LX, Xu F, Ma YG, Ong CK. Structure and magnetic characterizations of cobalt ferrite films prepared by spray pyrolysis. *Thin Solid Films* 2009, **517**: 5858-5861.

[61] Warren FJ, Gidley MJ, Flanagan BM. Infrared spectroscopy as a tool to characterise starch ordered structure—a joint FTIR–ATR, NMR, XRD and DSC study. *Carbohydr Polym* 2016, **139**: 35-42.

[62] Kim YI, Kim D, Lee CS. Synthesis and characterization of $CoFe_2O_4$ magnetic nanoparticles prepared by temperature-controlled coprecipitation method. *Physica B: Condens Matter* 2003, **337**: 42-51.

[63] Knobel M, Nunes WC, Socolovsky LM, *et al*. Superparamagnetism and Other Magnetic Features in Granular Materials: A Review on Ideal and Real Systems. *J Nanosci Nanotechnol* 2008, **8**: 2836-2857.

[64] Cullity BD, Graham CD. *Introduction to Magnetic Materials*. Wiley-IEEE Press, 2008.

[65] Batlle X, Labarta A. Finite-size effects in fine particles: magnetic and transport properties. *J Phys D* 2002, **35**: R15-R42.

[66] Linderoth S, Hendriksen PV, Bødker F, *et al*. On spin- canting in maghemite particles. *J Appl Phys* 1994, **75**: 6583-6585.

[67] Covaliu CI, Berger D, Matei C, et al. Magnetic nanoparticles coated with polysaccharide polymers for potential biomedical applications. *J Nanoparticle Res* 2011, **13**: 6169-6180.

[68] Dung TT, Danh TM, Hoa LTM *et al*. Structural and magnetic properties of starch-coated magnetite nanoparticles. *J Exp Nanosci* 2009, **4**: 259-267.

[69] Ayyappan S, Philip J, Raj B. Effect of Digestion Time on Size and Magnetic Properties of Spinel $CoFe_2O_4$ Nanoparticles. *J Phys Chem C* 2009, **113**: 590-596.

[70] Finsy R. On the Critical Radius in Ostwald Ripening. *Langmuir* 2004, **20**: 2975-2976.

[71] Lu HM, Zheng WT, Jiang Q. Saturation magnetization of ferromagnetic and ferrimagnetic nanocrystals at room temperature. *J Phys D* 2007, **40**: 320-325.

[72] Sharifi Dehsari H, Asadi K. Impact of Stoichiometry and Size on the Magnetic Properties of Cobalt Ferrite Nanoparticles. *J Phys Chem C* 2018, **122**: 29106-29121.

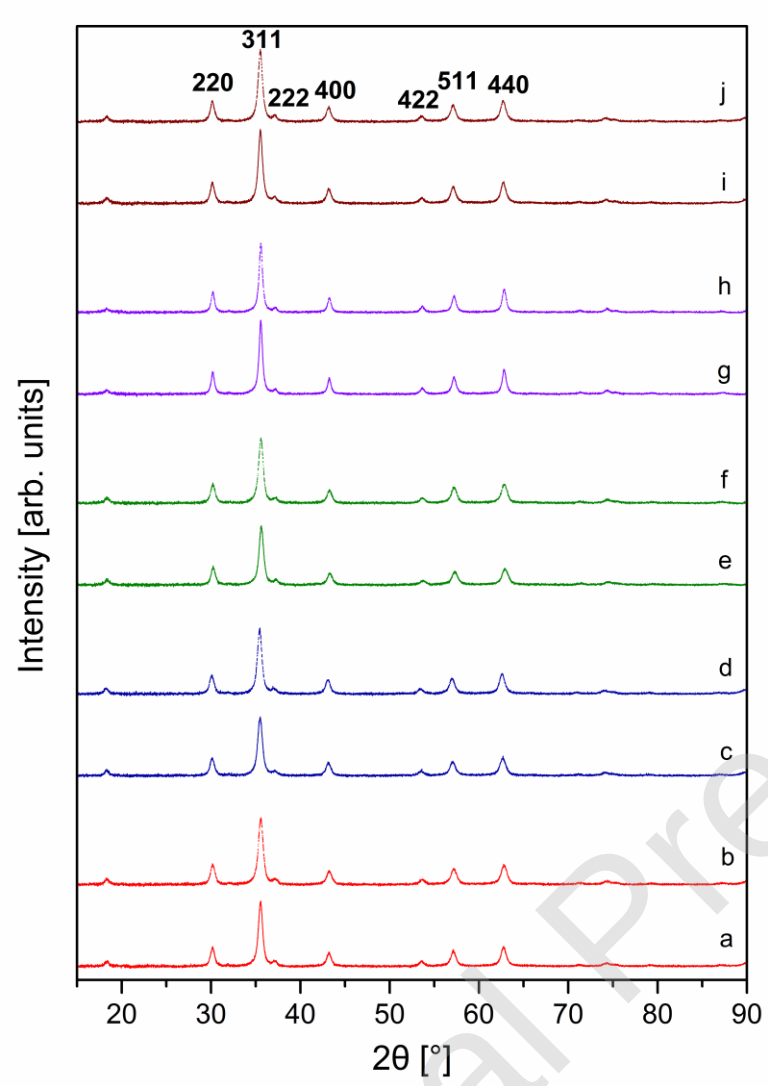


**Figure 1.** Collected XRPD patterns of uncoated and starch-coated cobalt ferrites. $CoFe_2O_4$ prepared by a) coprecipitation method, b) coprecipitation method/starch coating, c) mechanochemical method, d) mechanochemical method/starch coating, e) ultrasonically **assisted** coprecipitation method, f) ultrasonically assisted coprecipitation method/starch coating, g) microemulsion method, h) microemulsion/starch coating, i) microwave-assisted hydrothermal method, and j) microwave-assisted hydrothermal method/starch coating.

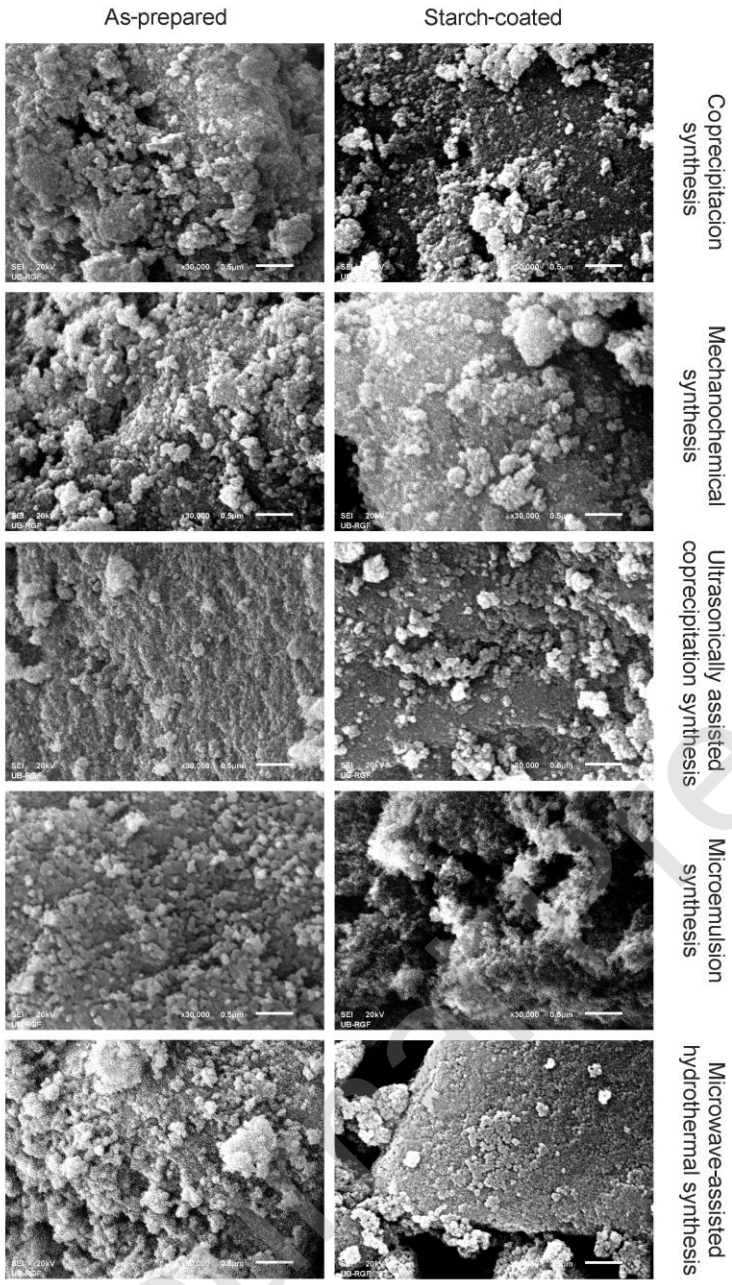


**Figure 2.** SEM analysis of the synthesized cobalt ferrites.

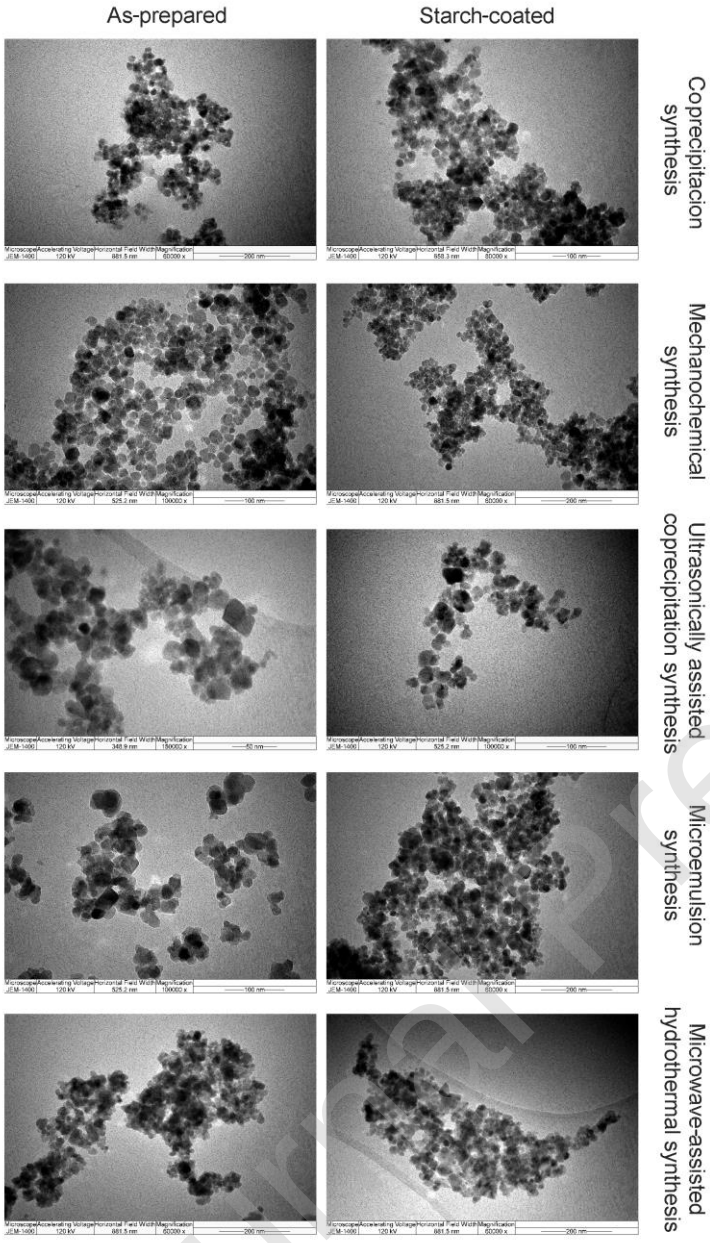


**Figure 3.** TEM analysis of the synthesized cobalt ferrites.

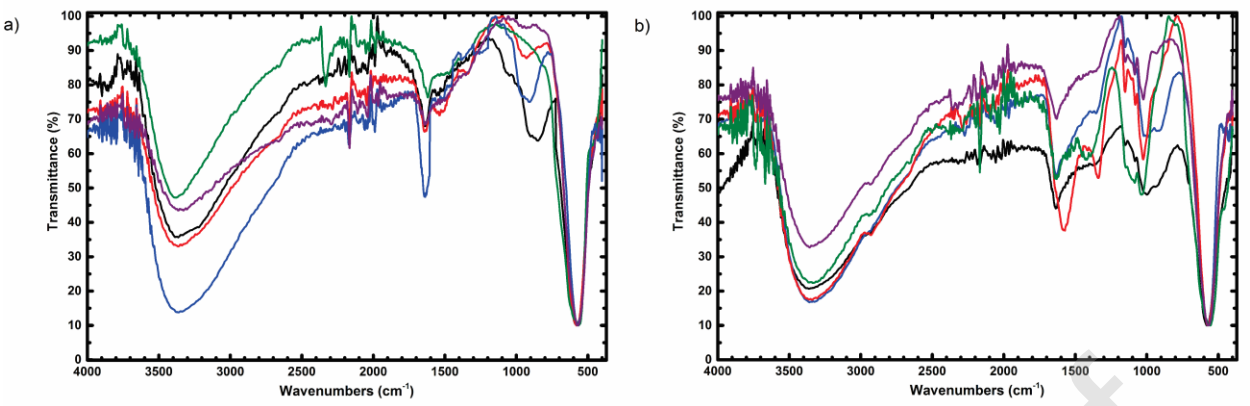


**Figure 4.** FT-IR spectra of a) as-prepared and b) starch-coated $CoFe_2O_4$ particles prepared by: the coprecipitation method (black), mechanochemical method (blue), ultrasonically assisted coprecipitation method (red), microemulsion method (green) and microwave-assisted hydrothermal method (purple).

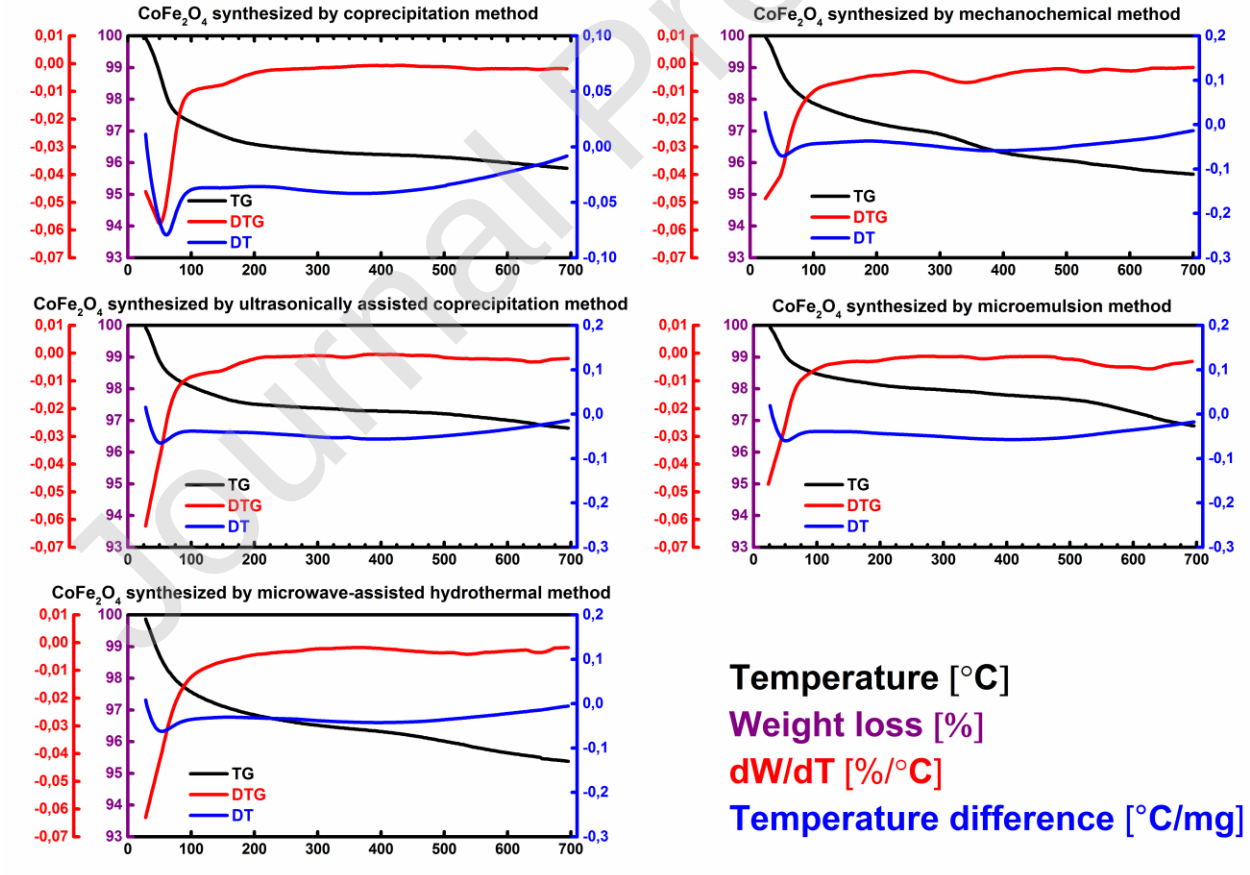

**Figure 5.** TG, DTG and DT curves for the as-prepared $CoFe_2O_4$ samples.

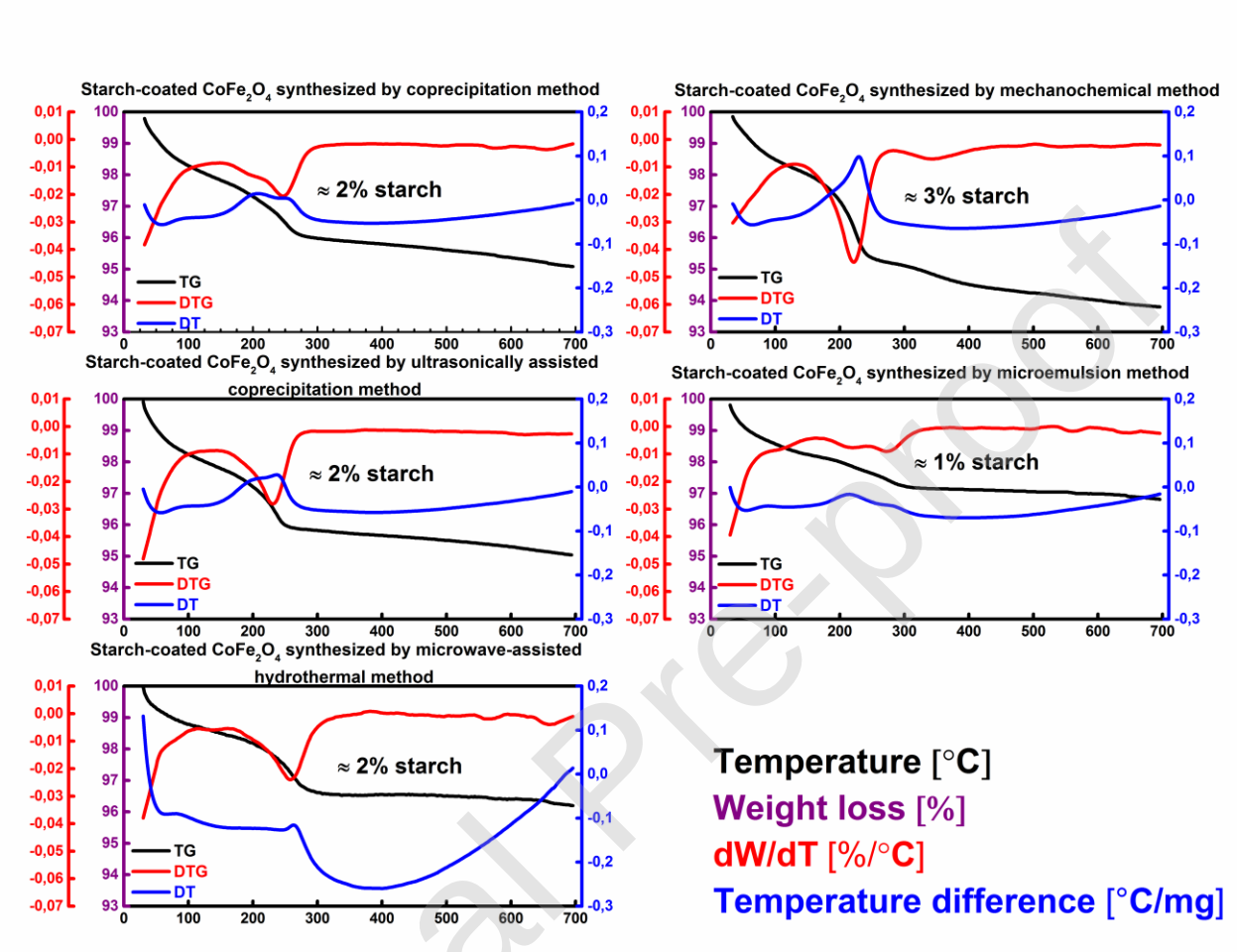


**Figure 6.** TG, DTG and DT curves for the starch-coated $CoFe_2O_4$ samples.

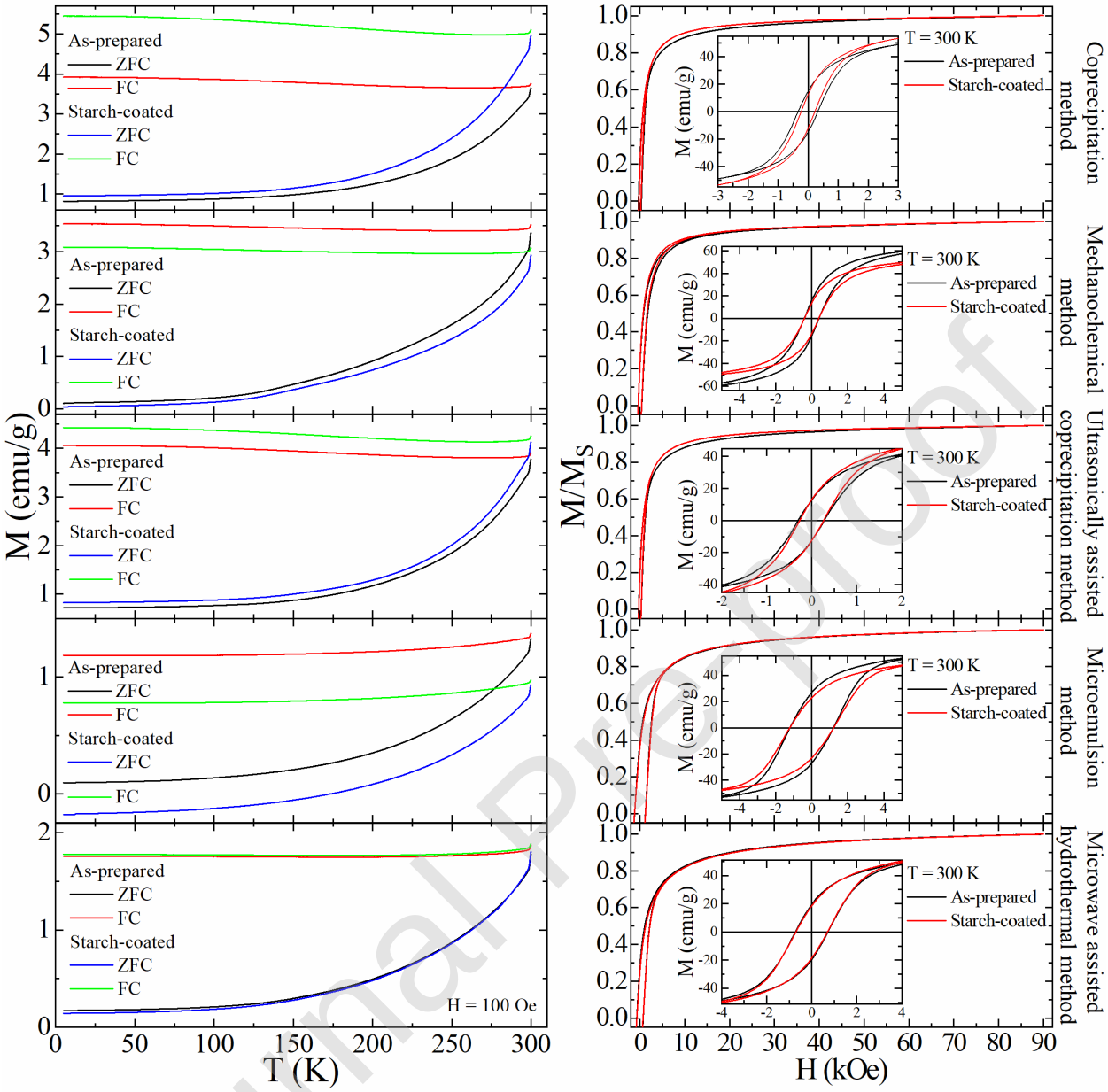


**Figure 7.** Results of the magnetization measurements obtained for the synthesized samples including (i) magnetization as a function of temperature measured at $H$ = 100 Oe with the sample being cooled in the absence (ZFC) and the presence (FC) of the magnetic field $H$ = 100 Oe and (ii) magnetization as a function of the magnetic field measured at $T$ = 300 K.

**Table 1.** Results of Rietveld refinement (the weighted profile R-factor ($R_{wp}$), the unweighted profile R-factor ($R_p$), the statistically expected R value ($R_{exp}$) and $\chi^2$ value)

| $CoFe_2O_4$ prepared by | $R_{wp}$ | $R_p$ | $R_{exp}$ | $\chi^2$ |
|---|---|---|---|---|
| Coprecipitation method | 2.16 | 1.71 | 2.25 | 0.93 |
| Coprecipitation method* | 2.18 | 1.71 | 2.19 | 0.98 |
| Mechanochemical method | 2.16 | 1.70 | 2.27 | 0.90 |
| Mechanochemical method* | 2.12 | 1.67 | 2.21 | 0.92 |
| Ultrasonically assisted coprecipitation method | 2.14 | 1.68 | 2.24 | 0.91 |
| Ultrasonically assisted coprecipitation method* | 2.13 | 1.68 | 2.22 | 0.92 |
| Microemulsion method | 2.55 | 1.99 | 2.49 | 1.02 |
| Microemulsion method* | 2.67 | 2.06 | 2.55 | 1.1 |
| Microwave assisted hydrothermal method | 2.15 | 1.69 | 2.21 | 0.95 |
| Microwave assisted hydrothermal method* | 2.28 | 1.79 | 2.23 | 1.05 |

*starch-coated

**Table 2.** Unit cell parameters (Å), volumes ($Å^3$) and microstructural parameters for the investigated cobalt ferrites

| $CoFe_2O_4$ prepared by | Unit cell parameter (Å) | Volume ($Å^3$) | Crystallite Size (nm) | Microstrain (%) |
|---|---|---|---|---|
| Coprecipitation method | 8.3723(5) | 586.98(7) | 12.0±1.2 | 0.32(6) |
| Coprecipitation method* | 8.3738(5) | 587.17(7) | 12.1±1.6 | 0.44(3) |
| Mechanochemical method | 8.3845(5) | 589.42(7) | 11.3±1.9 | 0.39(5) |
| Mechanochemical method* | 8.3888(4) | 590.34(6) | 12.5±0.9 | 0.37(2) |
| Ultrasonically assisted coprecipitation method | 8.3558(6) | 583.40(8) | 11.9±1.5 | 0.54(2) |
| Ultrasonically assisted coprecipitation method* | 8.3616(5) | 584.61(6) | 13.9±1.8 | 0.37(4) |
| Microemulsion method | 8.3610(4) | 584.49(5) | 12.8±1.8 | 0.15(4) |
| Microemulsion method* | 8.3628(4) | 584.87(5) | 14.3±1.2 | 0.11(5) |
| Microwave assisted hydrothermal method | 8.3738(4) | 587.18(6) | 12.5±1.9 | 0.41(4) |
| Microwave assisted hydrothermal method* | 8.3785(5) | 588.17(6) | 15.0±1.9 | 0.52(2) |

*starch-coated

**Table 3.** Weight percentage of elements (Co, Fe) in as-prepared and starch-coated $CoFe_2O_4$ samples obtained by EDS analyses

| Preparation method | Element | As-prepared Wt % | Starch-coated Wt % |
|---|---|---|---|
| Coprecipitation | Co | 29.75 | 35.15 |
| | Fe | 67.71 | 64.85 |
| Mechanochemical | Co | 33.78 | 33.39 |
| | Fe | 66.22 | 63.87 |
| Ultrasonically assisted coprecipitation | Co | 39.19 | 35.10 |
| | Fe | 60.81 | 64.25 |
| Microemulsion | Co | 27.92 | 32.25 |
| | Fe | 68.38 | 67.75 |
| Microwave assisted hydrothermal | Co | 35.31 | 33.51 |
| | Fe | 64.69 | 66.49 |

*oxygen is stoichiometrically normalized

**Table 4.** IR assignments for $CoFe_2O_4$ particles prepared by: the coprecipitation method (A), mechanochemical method (B), ultrasonically assisted coprecipitation method (C), microemulsion method (D) and microwave assisted hydrothermal method (E)

| *Wavenumbers for uncoated particles ($cm^{-1}$)* | | | | | *Assignments* |
|---|---|---|---|---|---|
| A | B | C | D | E | |
| 3367 | 3372 | 3361 | 3388 | 3361 | Stretching vibrations of water |
| 1635 | 1640 | 1630 | 1613 | 1633 | Bending vibrations of water |
| 558 | 574 | 580 | 563 | 559 | $Fe_{tetra}$-O |
| 417 | 423 | 428 | 439 | 428 | $Co_{octa}$-O |
| *Wavenumbers for coated particles ($cm^{-1}$)* | | | | | |
| 3363 | 3359 | 3339 | 3329 | 3332 | Hydrogen bonded OH stretching |
| 2931 | 2936 | 2920 | 2941 | 2931 | CH and $CH_2$ stretching |
| 1636 | 1628 | 1574 | 1629 | 1633 | Bending vibrations of water |
| 1454 | 1460 | 1461 | 1421 | 1465 | $CH_2$ bending in plane |
| 1351 | 1340 | 1335 | 1381 | 1362 | CH bending in plane |
| 999 | 996 | 1025 | 1039 | 1020 | COH stretching |
| 922 | 912 | 925 | 927 | 925 | C-O-C stretching |
| 580 | 576 | 573 | 558 | 575 | $Fe_{tetra}$-O |
| 430 | 426 | 400 | 428 | 412 | $Co_{octa}$-O |

*The uncertainty of the method with a 95% confidence interval is 0.2 $cm^{-1}$

**Table 5.** The magnetization (*M*s) at 90 kOe and nonzero coercive field (*H*c) values for all investigated samples

| $CoFe_2O_4$ prepared by | As-prepared | | Starch coated | |
|---|---|---|---|---|
| | $M_S$ (emu/g) | $H_C$ (Oe) | $M_S$ (emu/g) | $H_C$ (emu/g) |
| Coprecipitation method | **66.4(1)** | 329(8) | **69.9(1)** | 231(4) |
| Mechanochemical method | **72.1(1)** | 407(2) | **59.0(1)** | 400(6) |
| Ultrasonically assisted coprecipitation method | **61.9(1)** | 291(12) | **66.0 (1)** | 265(1) |
| Microemulsion method | **69.5 (1)** | 1206(7) | **62.6 (1)** | 1219(1) |
| Microwave assisted hydrothermal method | **69.7(1)** | 723(1) | **72.9(1)** | 702(1) |